Optimizing lateral homogeneity of ion-induced surface modifications of non-planar dielectric polyethylene components employing ion fluence simulations and optical measurements of the sp2-dependent reflectivity

Jochen Taiber[1], Sascha Buchegger[1], Bernd Stritzker[1], Achim Wixforth[1,2,3], and Christoph Westerhausen[1,2,3]

[1] Chair for Experimental Physics 1, University of Augsburg, Augsburg 86159, Germany
[2] Center for NanoScience (CeNS), Ludwig-Maximilians-Universität Munich, 80799 Munich, Germany
[3] Augsburg Center for Innovative Technologies (ACIT), Augsburg 86159, Germany
***** Correspondence: christoph.westerhausen@gmail.com; Tel.: +49-821-598-3311

***Abstract* — An approach to enhance the durability of artificial joint replacements is to modify the surface of their polymeric bearing material to diamond-like carbon (DLC) by ion-induced polymer-to-DLC-transformation in a plasma-immersion ion implantation process. Due to the dielectric character of the polymer and thus the impossibility of direct application of high voltage pulses to the component, this process requires an additional accelerator electrode above the surface. We here present two useful tools to optimize the geometry of such electrodes. First, we simulate the ions' trajectories for various electrode geometries and receive the resulting fluence distribution across the surface of the treated part. Second, we introduce a novel optical method to determine non-destructively the local ratio of sp^2 hybridized carbon atoms and thus the locally implanted fluence utilizing changes in reflectivity. Combining both tools, we here optimize, by way of example, the geometry of a grid electrode to obtain a homogeneous DLC-modification of a typical hip replacement inlay.**

1. Introduction

Representing the sixth most frequent surgery in Germany in 2016, the implantation of a hip total endoprosthesis was performed more than 230,000 times [1]. Considering the demographic change - the share of citizens of the overall population at the age of 65 and older will increase from 21% in 2013 to 33% in 2060 [2] - and the average age for primary total hip joint replacements (currently 69.7 years [3]), the interest in increasing the life span of an artificial joint replacement is clearly visible. The service life in today's joint replacement amounts to 15 to 20 years which explains the quantity of about 47,000 revision surgeries (hip + knee) in 2014 in Germany [4]. Aseptic loosening accounts for more than two thirds of all failing issues and is mainly caused by wear debris increasing the activity of macrophages and osteoclasts and ending up in enhanced osteolysis and thereby loosening of the implant [5].

Considering the amount of wear particles, a major step has been taken by using highly cross-linked polyethylene as inlay material in combination with a ceramic joint head [6–8]. Further progress could be possible with the application of diamond-like carbon (DLC); an amorphous modification with a significant portion of sp^3 hybridized carbon atoms (at least 10%) showing high hardness, excellent biocompatibility and low surface roughness [9,10].

Therefore, DLC coatings are used in a broad range of industrial applications: Especially its outstanding tribological properties qualify it for bearings, sliding surfaces and protective coatings, e.g. in the automotive industry, for magnetic storage media or, as mentioned, in a medical context [11]. In principal, the metastable DLC is prepared under ion bombardment of the growing film [12]. The desired film composition and thus its properties strongly depend on the deposition method which can mainly be categorized in PVD (physical vapor deposition) and PECVD (plasma-enhanced chemical vapor deposition) techniques. Hydrogenated forms of DLC (a-C:H) can be produced in a PECVD process in which the vapour deposition occurs due to chemical reactions on the substrate. The required energy is provided by a plasma which thus allows much lower process temperatures compared to common CVD [12–14]. In contrast, hydrogen free amorphous carbon (a-C) and tetrahedral amorphous carbon (ta-C) films result from PVD where a carbon containing material is evaporated and the carbon ions are condensed to the substrate's surface. Common PVD processes are magnetron sputtering (often used in industrial applications), pulsed laser deposition or vacuum arc evaporation [10,15–18].

Another appropriate way of realizing diamond-like properties is the ion bombardment of a polymeric base material leading to densification, hydrogen loss and cross-linking of the carbon network and finally resulting in a DLC modification of the surface layer up to a depth of about 300 nm [19,20]. Compared to common coatings, the risk of delamination is strongly reduced due to the decreased layer tension as result of the range distribution of the ions and thus a gradient in hardness and density [21,22]. A further benefit is the easy integration of antibacterial properties by implanting metal nanoparticles [23].

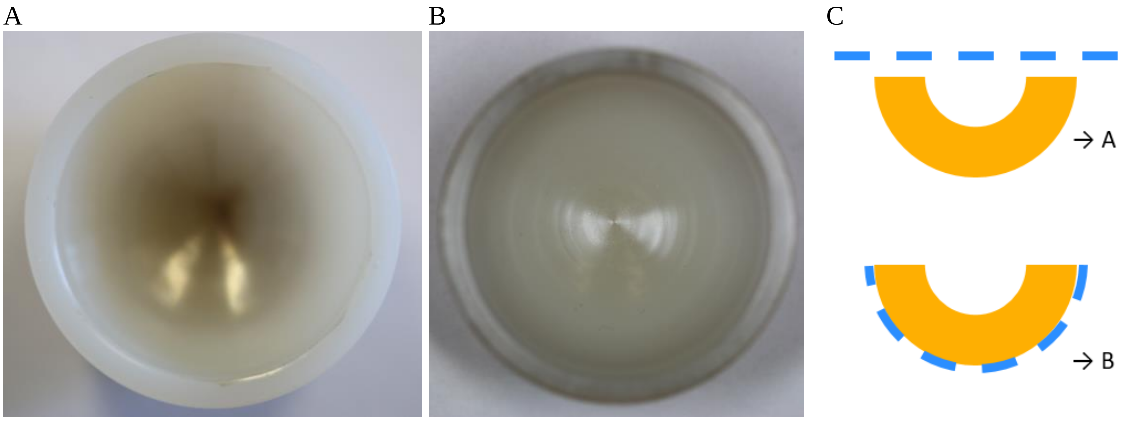

FIG 1: Modification of non-planar samples A) Inhomogeneous surface modification using a flat top-side grid-electrode B) Homogeneous modification using a backside-electrode. C) Illustration of flat top and curved backside electrode.

Ion implantation in electrically conducting objects using Plasma Immersion Ion Implantation is easily possible [24]. On the contrary, surface modifications of an insulating polymer can either be performed by using an additional cathode above the surface or at the sample's backside. This can be realized in a simple way for planar samples. However, complex-shaped objects require greater effort, especially if the use of a back-side electrode is not possible due to a variation of the sample thicknesses resulting in a variation of the effective electrical field. Because of the dependence on the orientation of the surface according to the moving direction of the accelerated ions, DLC modification becomes inhomogeneous for non-planar components in the case of a flat grid cathode (see fig. 1 a)). Therefore, the geometry of the electrode has to be optimized for each specific sample geometry.

To do so, we simulated the ions' trajectories using different geometries of the grid electrode to gain the implanted ion density on the surface of the implant. Using the developed simulation, we optimized the electrode shape for homogeneous surface modification of a hip inlay. As a second step, we introduced a novel optical method to determine non-destructively and space-resolved the ion fluence locally implanted into complex shaped surfaces. Based on the measurement of the local reflectivity which varies according to the local ratio of sp^2 hybridized carbon atoms, this method allows to measure the implanted ion fluence and thus gives information about the homogeneity of the surface modification. Combining simulation and optical examination, it is possible to optimize the geometry of the grid electrode for homogeneous modification adapted to the shape of the component.

2. Materials and methods

DLC

As primary material we used a highly cross-linked Ultra High Molecular Weight Polyethylene (UHMWPE) which is vitamin E stabilized (Vitelene®, Aesculap AG, Germany) [25,26] and has a molecular mass of about 5000 kg/mol before irradiation [27].

We transformed the surface of the polymer to DLC by implanting ions in a plasma immersion ion implantation step. Due to cross-linking, densification and a rearrangement of bonds, this process leads to the formation of a diamond-like carbon surface. For this process, we used a gas mixture of 20% Argon and 80% Hydrogen at a pressure of $p = 5 \cdot 10^{-3}$ mbar. We applied P_m = 800 W of microwave power (f = 2.45 GHz) to generate the plasma in an electron cyclotron resonance (ECR) plasma source. The ions of the plasma were accelerated towards the surface by applying a pulsed high voltage of V_p = 20 kV with a repetition rate of f_R = 20 Hz and a pulse width of τ = 5 µs to the electrode grid. Due to the range distribution of the impinging ions, the result is an about 300 nm thick surface near region of DLC with a gradient in hardness, density and diamond-like properties. This gradient reduces the internal stress and could be of great advantage for the adhesion of the DLC-surface and could therefore improve the long-time stability of the surface.

Simulation

To evaluate space-resolved the implanted fluence on the sample surface, we simulated the trajectories of the ions which are extracted from the plasma boundary sheath and accelerated towards the grid electrode, passing it and finally hitting the target's surface, as illustrated in fig. 2.

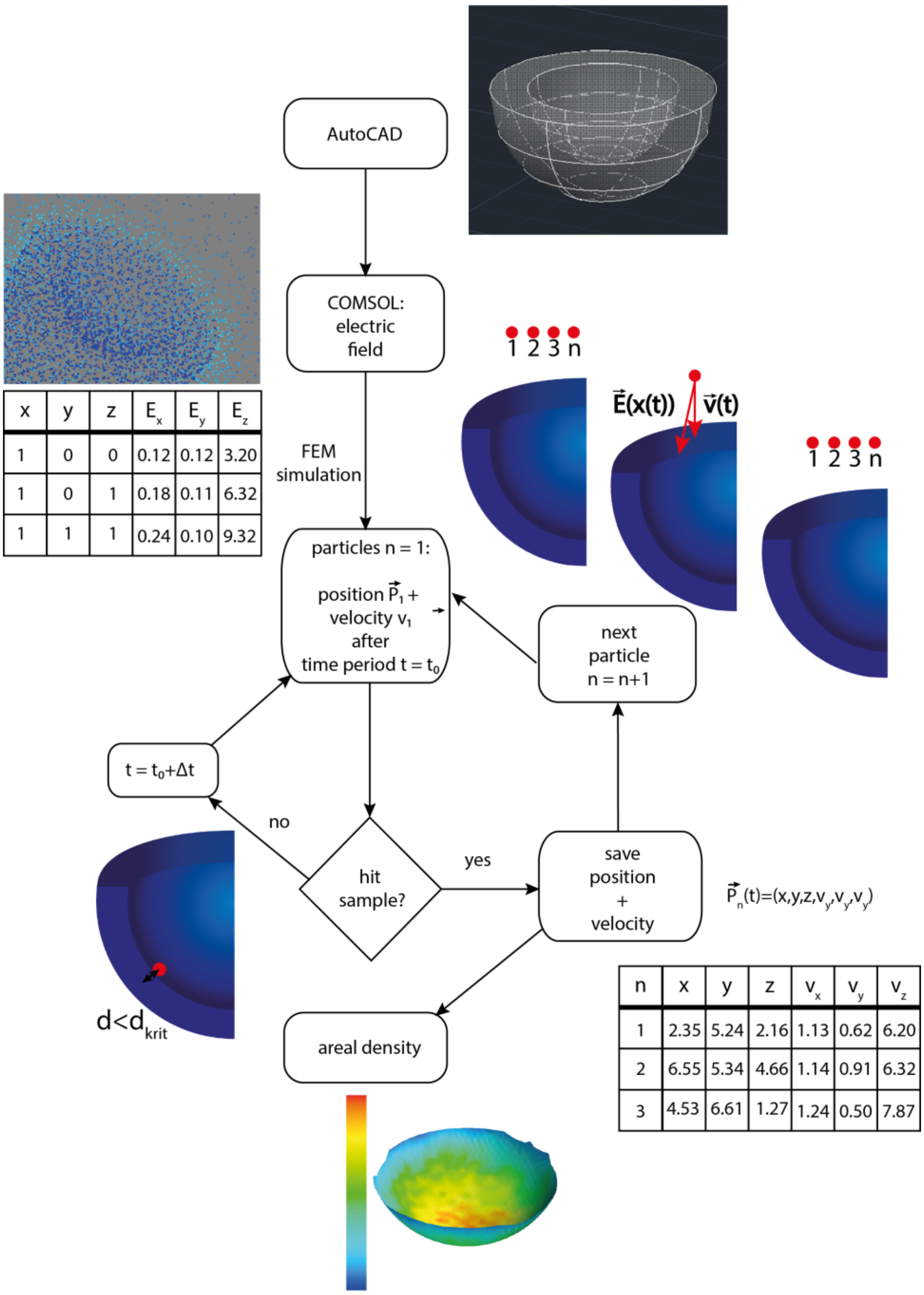

FIG 2: Schematic illustration of the simulation.

As first step, we modelled all components (inlay, grid electrode etc.) by using a common 3D computer-aided design software (Autodesk AutoCAD® 2017) which also makes it possible to integrate existing 3D models, for example a commercially available hip inlay. The plasma was simulated by an arrangement of positive charged particles with a median distance of 72 mm to the electrode. The median distance was estimated using Child's Law, which shows that the plasma sheet expands from 18 mm to 132 mm during a 5 µs lasting high voltage pulse. Because of the low impact of this distance on the ion trajectory, we simply assumed an intermediary distance of 72 mm. According to the experimental setup the mesh size of the grid cathode varied from 0.16 mm to 1.5 mm. However, above a distinct distance between electrode and sample, the grid characteristic of the anode can be neglected and the electrode can be replaced by a massive body which is penetrable by ions (see *3. Results: Grid shading*).

By utilizing a finite element tool (Comsol Multiphysics® 5.2.0.220 with AC/DC (electrostatics) and CAD Import module) we then simulated the electric field of the arrangement. To keep the computing time within an acceptable range, a physics-controlled mesh was used with higher point density on the sample to improve accuracy. The electric field as well as the geometries of the electrode and the sample were subsequently exported as a point cloud to a python script.

As first step of the script, a starting configuration was generated distributing the particles equally across the plasma boundary sheet (spherical or circular). The particle state at a point in time is defined as a vector with six components describing the position and the velocity of the particle: $\vec{p}_n = (x, y, z, v_x, v_y, v_z)$. For each particle and each time step, the nearest point of the electric field was identified by determining the distances to all other points. By means of this electric field value, the movement of the considered particle was calculated using suitable parameters (e.g. the corresponding ion mass). This was repeated as long as the distance between the particle and the electrode or sample has not fallen below the before defined minimum distance.

The evaluation of the results was implemented in two ways. For grasping all important information at a glance, a graphical approach was used performing a Delaunay triangulation of the sample's surface and assigning each triangle a distinct colour according to the calculated particle density at the corresponding position. For a more quantitative evaluation, we used two custom python analysis scripts to plot the particle density against its position on the sample's surface. As per default the script averages over either a rectangular interval (planar sample) or a 5°-segment of a spherical zone, depending on the geometry of the sample.

Optical measurement: ion-induced colour change

The optical measurement of the DLC modification is based on determining the reflectivity of the sample at a distinct wavelength interval. As can be seen in fig. 4 a), the higher the implanted fluence, the darker the surface appears. Furthermore, a yellowish tint occurs which transforms into a bronze colour at high fluences accompanied by an increasing metallic gloss [28]. The reason for this behaviour can be found in the bonding structure of the material: it is well known that the energy differences between molecular vibrations and rotations in usual polymers are too small and the differences between different electron states are too large for excitation within the visible range [29]. But the situation is different if there are delocalized π electrons. In this case, the energy gap between the highest occupied and the lowest unoccupied molecular orbital is decreasing which lowers the energy threshold and leads to an absorption of light with a larger wavelength.

In the polyethylene starting material, a large fraction of carbon atoms is sp^3 hybridized and bound to further carbon or hydrogen atoms via σ bonds. The DLC transformation increases the percentage of sp^2 hybridized carbon atoms resulting in a larger amount of π electrons. Inter alia, being arranged in olefinic or even forming entire sp^2 clusters, the delocalization of these π electrons becomes larger and larger [10,21,30]. Thus, the energy threshold decreases which allows absorption of blue light leading to the described yellowish tint of the sample and its darker appearance. According to the investigations of Schwarz-Selinger et al. [30], the compaction of the material during DLC transformation induces an increase in the refractive index. Dowling et al. [31] showed that this results in a higher extinction coefficient and thus in a higher reflection which explains the metal gloss of the DLC layer. We assume that, similar to the high mobility of the conduction electrons in metals, the delocalization of the π electrons in DLC layers hence plays the key role for the gloss. This description is in accordance to previous publications [32–34], but should not be further elaborated as this study focusses on employing this optical phenomenon to evaluate the implanted fluence.

Optical measurement: setup

To investigate complex-shaped objects, a flexible setup with high reproducibility is necessary. Thus, we chose a reflectivity measurement via optical fibres to enable examinations in any orientation without having to take care of the illumination of the sample. As can be seen in fig. 3, the light from the light source (LED or Xenon lamp) was coupled into a reflection probe

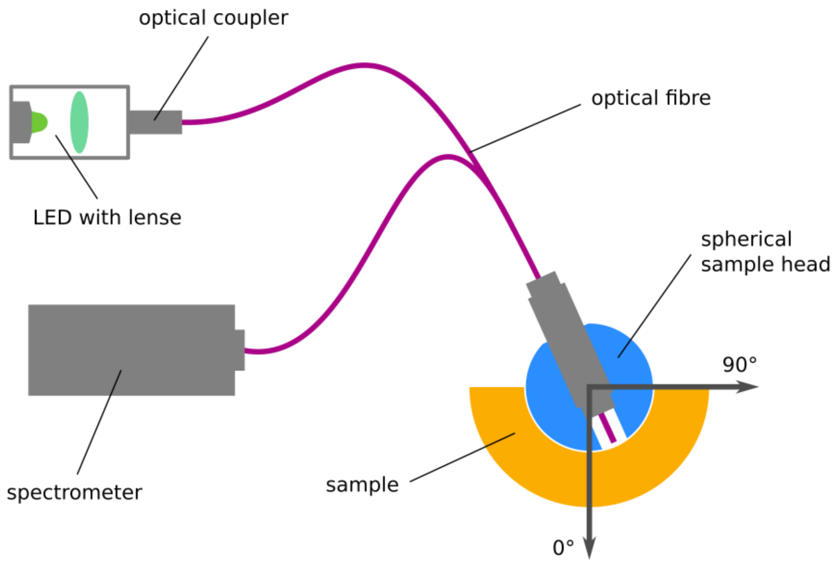

FIG 3: Illustration of the optical measurement of the local reflectivity as a measure for the local applied fluence.

(Thorlabs RP22) which was connected to a sample head, here in a spherical shape made of a ceramic femoral head. Thus, it was possible to keep the distance between the end of the fibre and the surface of the sample very constant which is indispensable for accurate measurements. The intensity of the reflected radiation was detected by a spectrometer (Ocean Optics QE65000) or a power meter (Thorlabs PM100D / S150C).

3. Results

Spectral Range

For choosing an appropriate spectral range, we first recorded spectra between 400 nm and 1000 nm using five different standard samples (CNC-milled UHMWPE wafers having a diameter of 10 mm), treated with fluences of 2•10^{17} cm^{-2}, 1•10^{17} cm^{-2}, 5•10^{16} cm^{-2}, 1•10^{16} cm^{-2} and 0 cm^{-2} (no treatment). The resulting values were normalized using the values of light reflected by a mirror to eliminate the influence of the emission and are shown in fig. 4. By plotting the reflectance as function of the fluence for a distinct wavelength, a calibration curve can be obtained and fitted according to the equation $y = A \cdot e^{-\frac{x}{\tau}} + y_0$ .This way, it is possible to directly translate the measured intensity data into fluence values.

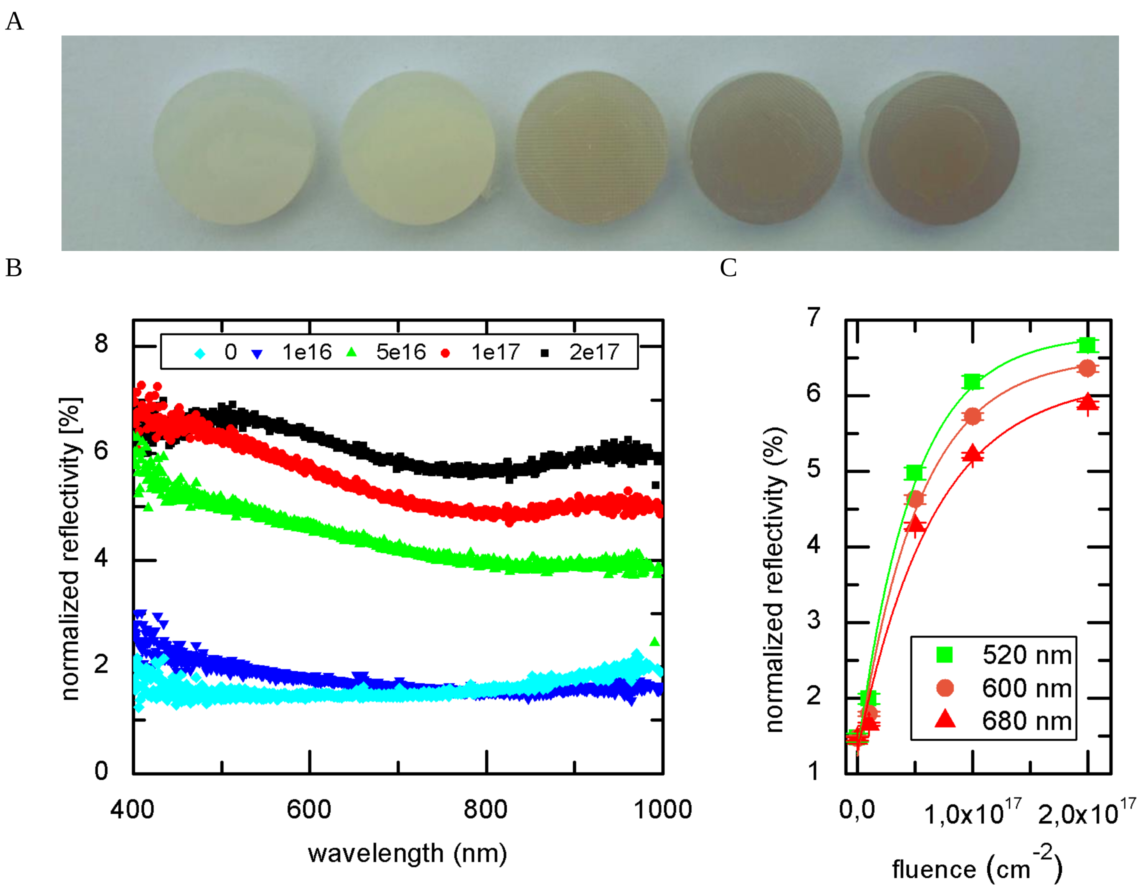

FIG 4: A) A colour change with increasing fluence is obvious. B) Reflectivity as function of wavelength for different fluences in units of cm^{-2}. C) Reflectivity as function of fluence for selected wave lengths fitted to exponential functions $y_{520nm} = -5.6\% \cdot e^{-\frac{x}{4.8\ 10^{16}}} + 6{,}8\%$, $y_{600nm} = -5.3\% \cdot e^{-\frac{x}{5.3\ 10^{16}}} + 6.5\%$ *and* $y_{680nm} = -4{,}8\% \cdot e^{-\frac{x}{5.5\ 10^{16}}} + 6.0\%$.

The reflectivity increases with increasing fluence until a saturation value is reached. Furthermore, it also slightly increases with decreasing wavelength which is consistent with the theoretical predictions. In the range between λ = 520 nm and λ = 700 nm conclusions about the fluence have the highest significance. Since in general the highest contrast can be observed at λ = 520 nm, we used a green high-power LED with a wavelength of λ = 518 nm for our measurements. To optimize the measurements for the high fluence regime higher wavelengths e.g. λ = 900 nm can be chosen.

Grid shading

To demonstrate the performance of the described optical measurement method, we modified cylindrical UHMWPE samples (thickness 2 mm, diameter 1mm) using a coarse grid (mesh size w = 1.5 mm, wire diameter d_w = 0.7 mm) which was placed at an adjustable distance *d* to the sample's surface.

The corresponding samples are shown in fig. 5 b): at the bright positions no ions reached the sample, whereas in the dark areas a DLC modification occurred. For the optical measurements we used a modified experimental setup where the fibre is fixed on a microscope stage and can be moved precisely in steps of 0.5 mm along the X and Y axes in constant distance of 0.5 mm to the surface. Figs. 5 c)-f) show the measured averaged fluence depending on the position on the sample in X direction. Obviously, there is a high level of agreement between the results determined by measuring the reflectance and the optical appearance of the samples shown in the photography.

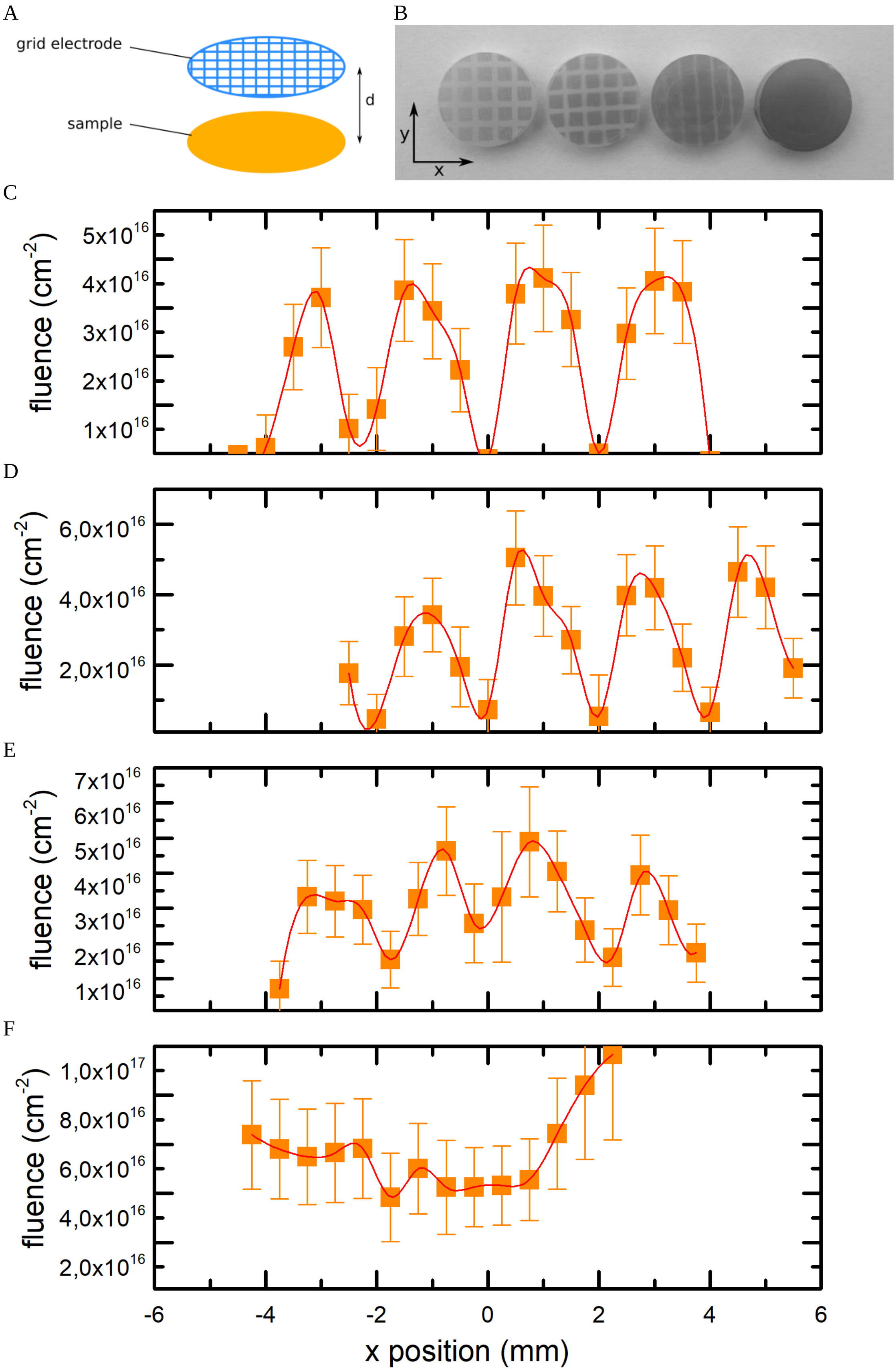

FIG 5: A) Illustration of the sample and mesh geometry B) Shadowing of the mesh during implantation for different fluences C)-F) Optical measurement of the implanted fluence

Measuring the reflectivity shows a width of the shadowing between 0.5 and 1 mm for the sample which has been modified with a sample to grid distance of 0 mm. This corresponds to the wire diameter and to the optical appearance of the sample shown in fig. 5 b). With increasing gap between sample and electrode, the resulting width of the shadow becomes gradually thinner and blurs until it nearly disappears at a distance of 50 mm. Above that distance, we therefore get a homogeneous surface modification with a constant fluence all over the surface of the sample. These results prove that the optical measurement of the sample's reflectivity is in accordance to the appearance of the sample and corresponds to the geometry of the sample and the electrode grid used in the experimental setup.

The simulation data (in fig. 6 shown for the 10-mm-case; in each case 10,000 particles simulated) also strongly support these findings. The peak positions are almost identical whereas the uncertainties are relatively high (about $2 \cdot 10^{16}$ cm^{-2}) in the measurement.

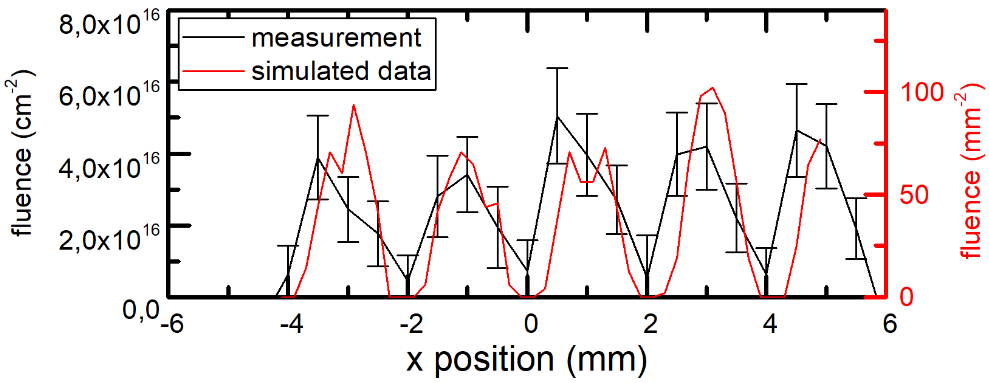

FIG 6: Simulated and measured implantation fluence for d=10 mm.

The latter could be explained by two influences: first, the accuracy of the optical measurements strongly depends on the smoothness of the surface. In our case we used samples with a comparatively rough surface ($R_A = 0.9$ µm) which corresponds to a typical roughness of polymer sliding surfaces in orthopaedic joint replacements, additionally affected by scratches from the CNC milling process. Second, the calibration curve (reflectivity as function of fluence) is significantly flatter for high fluences than for low ones. Consequently, measurements are much more sensitive in the low fluence regime. Nevertheless, the comparison of the simulated ion distribution and the measured fluence demonstrates that both methods are first in high accordance with each other and second in high accordance to the used experimental setup. This shows that we are able to cost-efficiently simulate the homogeneity of the treatment for any setup of sample and electrode. Furthermore, we can non-destructively measure the implanted fluence and therefore the homogeneity of the treatment.

Because of this coarse grid, primarily used for demonstration of the accuracy of the simulation and the optical measurement method, there is no relevant shading at relatively high distances above 50 mm between grid and sample. For the treatment of artificial joint components with plasma immersion ion implantation it is, however, more appropriate to use a finer grid electrode. Transferred to that which we used in the following experiments (mesh size of 0.16 mm, wire diameter of 0.112 mm), an electrode sample of about 5 mm is sufficient to prevent shading. To limit the required calculation time, we thus renounced modelling the full grid in the following simulations and replaced it by solid sheets that are assumed transparent for incoming particles.

Optimization of the implanted ion distribution for a joint inlay

In the following, we demonstrate, by way of example, the optimization of a hip inlay used as one part of the sliding surface in artificial joint replacements. The aim here is to homogeneously modify the component's surface to DLC and to optimize the geometry of the grid electrode for this purpose. Fig. 7 a) illustrates the use of a flat grid electrode above the hemispherical hip inlay which leads to strongly inhomogeneous results (Fig. 7b). Most of the ions are implanted in the centre where the surface is perpendicular to the moving direction of the particles and almost no implantation occurs on the outer area of the hip inlay. We therefore deformed the grid electrode in a way that it is equally spaced to the sample's surface. As can be seen from

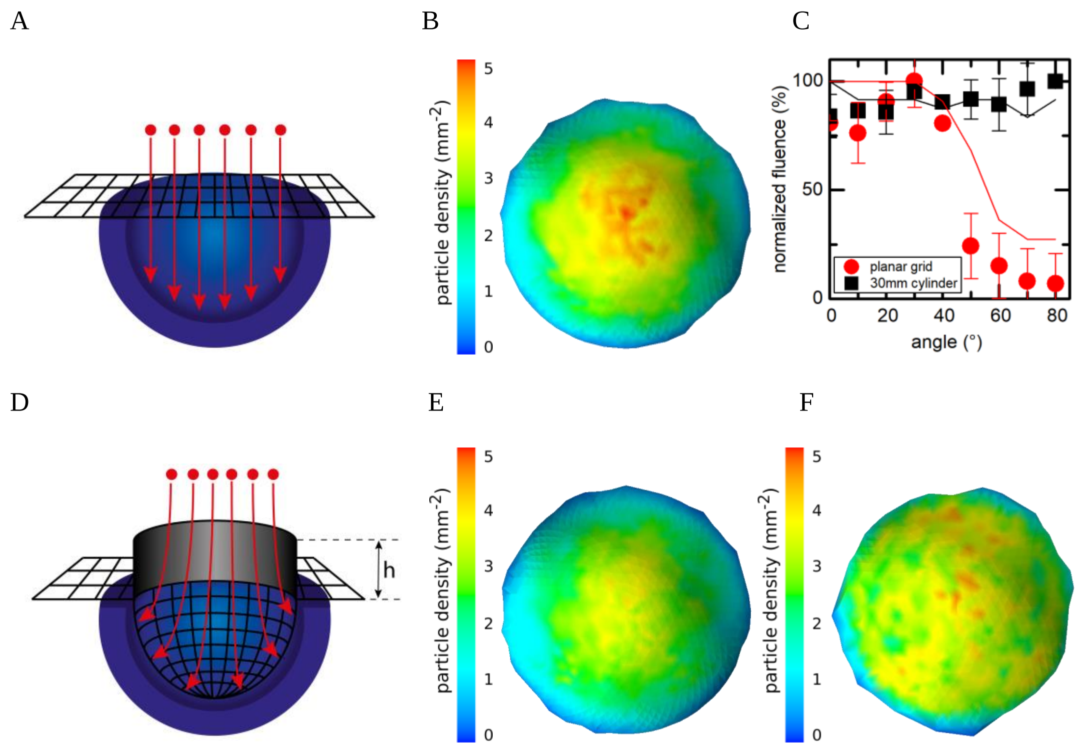

FIG 7: A) Illustration of the planar grid B) Simulated particle density after implantation C) Comparison of Simulation and measurement D) Illustration of a grid with additional cylinder of variable height E) Simulation of cylinder height h=0 mm and F) h=30 mm.

fig. 7 e), this electrode geometry shows almost the same result with a high fluence to the centre of the sample and almost no fluence on the outer area of the sample. To achieve ion implantation to the outer area of the hip inlay, a force directed radially outwards is necessary to deflect the ions. To get a radial force, we added a metallic hollow cylinder to the top of the mesh as shown in fig. 7 d). In the simulation, 21,600 ions are simulated and the height of the cylinder is varied from 0 mm (no cylinder) to 40 mm in steps of 5 mm (see Supporting Information). As shown in fig. 7 f), the fluence becomes most evenly distributed for a cylinder height of 30 mm which was experimentally verified by producing and measuring corresponding samples (see fig. 7 c)). This result is also consistent regarding the total number of particles hitting the sample's surface in the simulation: If the cylinder is higher than 30 mm, some particles are accelerated towards the shell of the cylinder and therefore the total number of particles hitting the sample's surface decreases for higher cylinders. If the cylinder is lower, the treatment becomes inhomogeneous. Therefore, the optimal height of the cylinder is 30 mm, leading to relatively homogeneous results.

Based on the above shown high correlation of simulations and experimental data, we simulated and analysed a spherical electrode structure as shown in fig. 8: a hemispherical grid is spherically continued and fixed to a thin mount. The idea is that the plasma boundary sheet can spread undisturbed around the electrode so that the trajectories of the ions run perpendicular to the surface. Considering the simulation results (see fig. 8; 22,000 particles simulated), this setup results in a highly homogenous DLC modification over the whole relevant surface of the joint inlay, differences in fluence are negligibly small. Therefore, we propose the use of a spherical grid electrode to homogeneously modify the surface of a UHMWPE hip inlay to DLC.

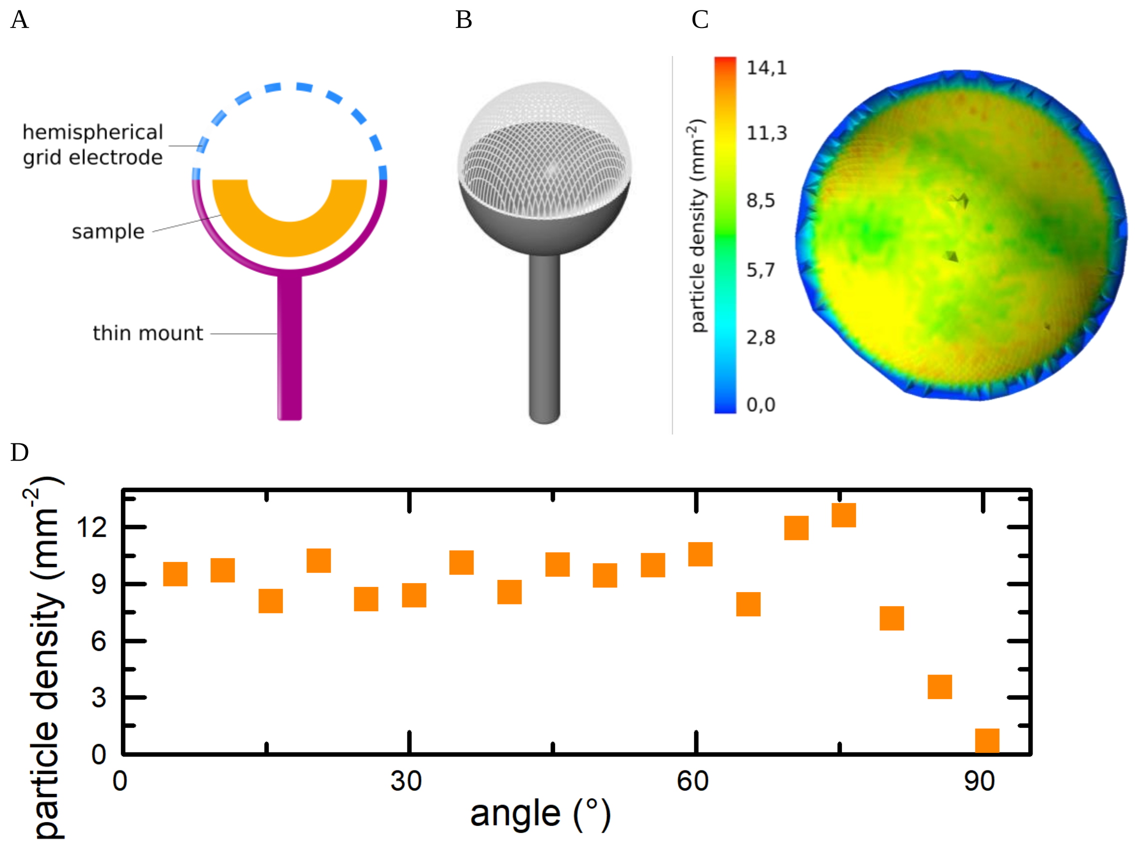

FIG 8: A)+B) Illustration of the hemispherical electrode setup C)+D) Simulation using a hemispherical electrode.

4. Conclusion

Considering complex-shaped dielectric parts for the homogeneous modification to diamond-like carbon, it is not possible to apply a high voltage directly. Thus, it is necessary to design a complex-shaped electrode which is placed above the surface. We therefore deliver two tools to optimize such grid electrodes.

First, we implemented a three-dimensional simulation process based on finite element analysis software and python scripts to calculate and visualize the ion density on the sample's surface which is a measure for DLC modification. The simple integration of diverse 3D CAD models enables a fast evaluation of multiple electrode geometries without the need of physically producing each of them. Thus, we are able to fast and cost-efficiently optimize the needed electrode for various sample geometries and particle types.

Second, for example, for the verification it is however required to judge the actually implanted ion density. Thus, we developed an optical measurement method to determine non-destructively the local ratio of sp² hybridized carbon atoms from which the degree of modification can be deduced. It is based on a reflectivity measurement via an optical fibre to ensure flexibility even for complex-shaped surfaces.

Combining both approaches, we demonstrate, by way of example, the optimization of the DLC modification of an UHMWPE joint inlay. We show that the surface modification of such an implant can be achieved by using either a combination of a mesh and a cylinder on top or by using a spherical electrode. Both setups lead to relatively homogeneous surface treatment, whereas the application of the spherical electrode leads to a slightly higher homogeneity.

A promising approach is the combination of our optical setup with a robotic arm which enables an automation of the measurement process and improves the results by ensuring a constant distance between the optical head and the surface of the sample. Using LEDs with various wavelengths to increase the sensitivity according to the fluence range, it is thus conceivable to apply this method in non-destructive quality assurance in the industrial environment.

In summary, we here deliver two useful tools for the DLC transformation of non-planar and insulating UHMWPE parts like joint replacement components.

Disclosures

The authors have no financial conflicts of interest.

Acknowledgments

The authors thank the “Deutsche Forschungsgemeinschaft (DFG)” for the financial support of this work under the contract “Erkenntnistransferprojekt Antibakterielle und abriebarme Beschichtung von Gleitflächen in orthopädischen Implantaten”. Moreover, the authors thank Matthias Weiß and Malina Reitemeyer for technical assistance.

References

1. Statistisches Bundesamt (Destatis). Die 20 häufigsten Operationen: Vollstationär behandelte Patientinnen und Patienten in Krankenhäusern 2016; 2017.
2. Statistisches Bundesamt (Destatis). Bevölkerung Deutschlands bis 2060: 13. koordinierte Bevölkerungsvorausberechnung; 2015.
3. Böhm K, Tesch-Römer C, Ziese T, editors. Gesundheit und Krankheit im Alter. Berlin: Robert Koch-Inst; 2009. (Beiträge zur Gesundheitsberichterstattung des Bundes). ger.
4. Bleß H-H, Kip M. Weißbuch Gelenkersatz. Berlin, Heidelberg: Springer Berlin Heidelberg; 2017.
5. Abu-Amer Y, Darwech I, Clohisy JC. Aseptic loosening of total joint replacements: Mechanisms underlying osteolysis and potential therapies. Arthritis Res Ther. 2007;9 Suppl 1S6. doi:10.1186/ar2170
6. Kaddick C, Catelas I, Pennekamp PH, Wimmer MA. Verschleiss und aseptische Prothesenlockerung: Eine Bestandsaufnahme [Implant wear and aseptic loosening. An overview]. Der Orthopäde. 2009;38(8):690–7. ger. doi:10.1007/s00132-009-1431-9
7. Sundfeldt M, Carlsson LV, Johansson CB, Thomsen P, Gretzer C. Aseptic loosening, not only a question of wear: A review of different theories. Acta Orthop. 2006;77(2):177–97. doi:10.1080/17453670610045902
8. Semlitsch, M., Lehmann, M., Weber, H., Doerre, E., & Willert, H. G. New prospects for a prolonged functional life-span of artificial hip joints by using the material combination polyethylene/aluminium oxide ceramic/metal. Journal of Biomedical Materials Research Part A. 1977;11(4).
9. Anne Thomson L, Law FC, Rushton N, Franks J. Biocompatibility of diamond-like carbon coating. Biomaterials. 1991;12(1):37–40. doi:10.1016/0142-9612(91)90129-X
10. Robertson J. Diamond-like amorphous carbon. Materials Science and Engineering: R: Reports. 2002;37(4-6):129–281. doi:10.1016/S0927-796X(02)00005-0
11. Hauert R. An overview on the tribological behavior of diamond-like carbon in technical and medical applications. Tribology International. 2004;37(11-12):991–1003. doi:10.1016/j.triboint.2004.07.017
12. Grill A. Diamond-like carbon: State of the art. Diamond and Related Materials. 1999;8(2-5):428–34. doi:10.1016/S0925-9635(98)00262-3
13. Fedosenko G, Schwabedissen A, Engemann J, Braca E, Valentini L, Kenny JM. Pulsed PECVD deposition of diamond-like carbon films. Diamond and Related Materials. 2002;11(3-6):1047–52. doi:10.1016/S0925-9635(01)00612-4
14. Unger E. Die Erzeugung dünner Schichten. Das PECVD-Verfahren: Gasphasenabscheidung in einem Plasma. Chemie in unserer Zeit. 1991;25(3):148–58. doi:10.1002/ciuz.19910250306
15. Bonelli M, Ferrari AC, Fioravanti A, Li Bassi A, Miotello A, Ossi PM. Structure and mechanical properties of low stress tetrahedral amorphous carbon films prepared by pulsed laser deposition. Eur. Phys. J. B. 2002;25(3):269–80. doi:10.1140/epjb/e20020031
16. Chowdhury S, Laugier MT, Rahman IZ. Characterization of DLC coatings deposited by rf magnetron sputtering. Journal of Materials Processing Technology. 2004;153-154804–10. doi:10.1016/j.jmatprotec.2004.04.265
17. Pappas DL, Saenger KL, Bruley J, Krakow W, Cuomo JJ, Gu T, Collins RW. Pulsed laser deposition of diamond-like carbon films. Journal of Applied Physics. 1992;71(11):5675–84. doi:10.1063/1.350501
18. Logothetidis S. Hydrogen-free amorphous carbon films approaching diamond prepared by magnetron sputtering. Appl. Phys. Lett. 1996;69(2):158–60. doi:10.1063/1.116906
19. Calcagno L, Compagnini G, Foti G. Structural modification of polymer films by ion irradiation. Nuclear Instruments and Methods in Physics Research Section B: Beam Interactions with Materials and Atoms. 1992;65(1-4):413–22. doi:10.1016/0168-583X(92)95077-5
20. Schwarz FP, Hauser-Gerspach I, Waltimo T, Stritzker B. Antibacterial properties of silver containing diamond like carbon coatings produced by ion induced polymer densification. Surface and Coatings Technology. 2011;205(20):4850–4. doi:10.1016/j.surfcoat.2011.04.078
21. Schwarz F, Thorwarth G, Stritzker B. Synthesis of silver and copper nanoparticle containing a-C: Hby ion irradiation of polymers. Solid State Sciences. 2009;11(10):1819–23. doi:10.1016/j.solidstatesciences.2009.05.012
22. Buchegger S, Schuster N, Stritzker B, Wixforth A, Westerhausen C. Multilayer diamond-like amorphous carbon coatings produced by ion irradiation of polymer films. Surface and Coatings Technology. 2017;32742–7. doi:10.1016/j.surfcoat.2017.08.010
23. Hauert R. A review of modified DLC coatings for biological applications. Diamond and Related Materials. 2003;12(3-7):583–9. doi:10.1016/S0925-9635(03)00081-5

24. Conrad JR, Radtke JL, Dodd RA, Worzala FJ, Tran NC. Plasma source ion-implantation technique for surface modification of materials. Journal of Applied Physics. 1987;62(11):4591–6. doi:10.1063/1.339055
25. Micheli BR, Wannomae KK, Lozynsky AJ, Christensen SD, Muratoglu OK. Knee simulator wear of vitamin E stabilized irradiated ultrahigh molecular weight polyethylene. J Arthroplasty. 2012;27(1):95–104. doi:10.1016/j.arth.2011.03.006
26. Aesculap Orthopaedics. Aesculap® Vitelene® Brochure O44301: Aesculap AG.
27. Quadrant MediTECH®. Data Sheet Chirulen® 1020-E; 21.01.2014.
28. Hartwig A. Umwandlung von ultrahochmolekularem Polyethylen in diamantähnlichen Kohlenstoff für den medizinischen Einsatz [Diploma Thesis]. Augsburg. 84 p. ger.
29. Meschede D. Gerthsen Physik. 24th ed. Berlin: Springer; 2010. (Springer-Lehrbuch). ger.
30. Prawer S, Nugent KW, Lifshitz Y, Lempert GD, Grossman E, Kulik J, Avigal I, Kalish R. Systematic variation of the Raman spectra of DLC films as a function of sp2: Sp3 composition. Diamond and Related Materials. 1996;5(3-5):433–8. doi:10.1016/0925-9635(95)00363-0
31. Schwarz-Selinger T, Keudell A v., Jacob W. Plasma chemical vapor deposition of hydrocarbon films: The influence of hydrocarbon source gas on the film properties. Journal of Applied Physics. 1999;86(7):3988–96. doi:10.1063/1.371318
32. Dowling DP, Donnelly K, Monclus M, McGuinness M. The use of refractive index as a measure of diamond-like carbon film quality. Diamond and Related Materials. 1998;7(2-5):432–4. doi:10.1016/S0925-9635(97)00233-1
33. Lifshitz Y. Diamond-like carbon — present status. Diamond and Related Materials. 1999;8(8-9):1659–76. doi:10.1016/S0925-9635(99)00087-4
34. Mednikarov B, Spasov G, Babeva T, Pirov J, Sahatchieva M, Popova C, Kulischa W. Optical properties of diamond-like carbon and nanocrystalline diamond films. Journal of Optoelectronics and Advanced Materials. 2005;7(3):1407–13.
35. Rangel EC, Cruz NCd, Kayama ME, Rangel RCC, Marins N, Durrant SF. Optical and Electrical Properties of Polymerizing Plasmas and Their Correlation with DLC Film Properties. Plasmas and Polymers. 2004;9(1):1–22. doi:10.1023/B:PAPO.0000039813.33634.c6

Supporting Information: Optimizing lateral homogeneity of ion-induced surface modifications of non-planar dielectric polyethylene components employing ion fluence simulations and optical measurements of the sp2-dependent reflectivity

Jochen Taiber[1], Sascha Buchegger[1], Bernd Stritzker[1], Achim Wixforth[1,2,3], and Christoph Westerhausen[1,2,3]

[1] Chair for Experimental Physics 1, University of Augsburg, Augsburg 86159, Germany
[2] Center for NanoScience (CeNS), Ludwig-Maximilians-Universität Munich, 80799 Munich, Germany
[3] Augsburg Center for Innovative Technologies (ACIT), Augsburg 86159, Germany
* Correspondence: christoph.westerhausen@gmail.com; Tel.: +49-821-598-3311

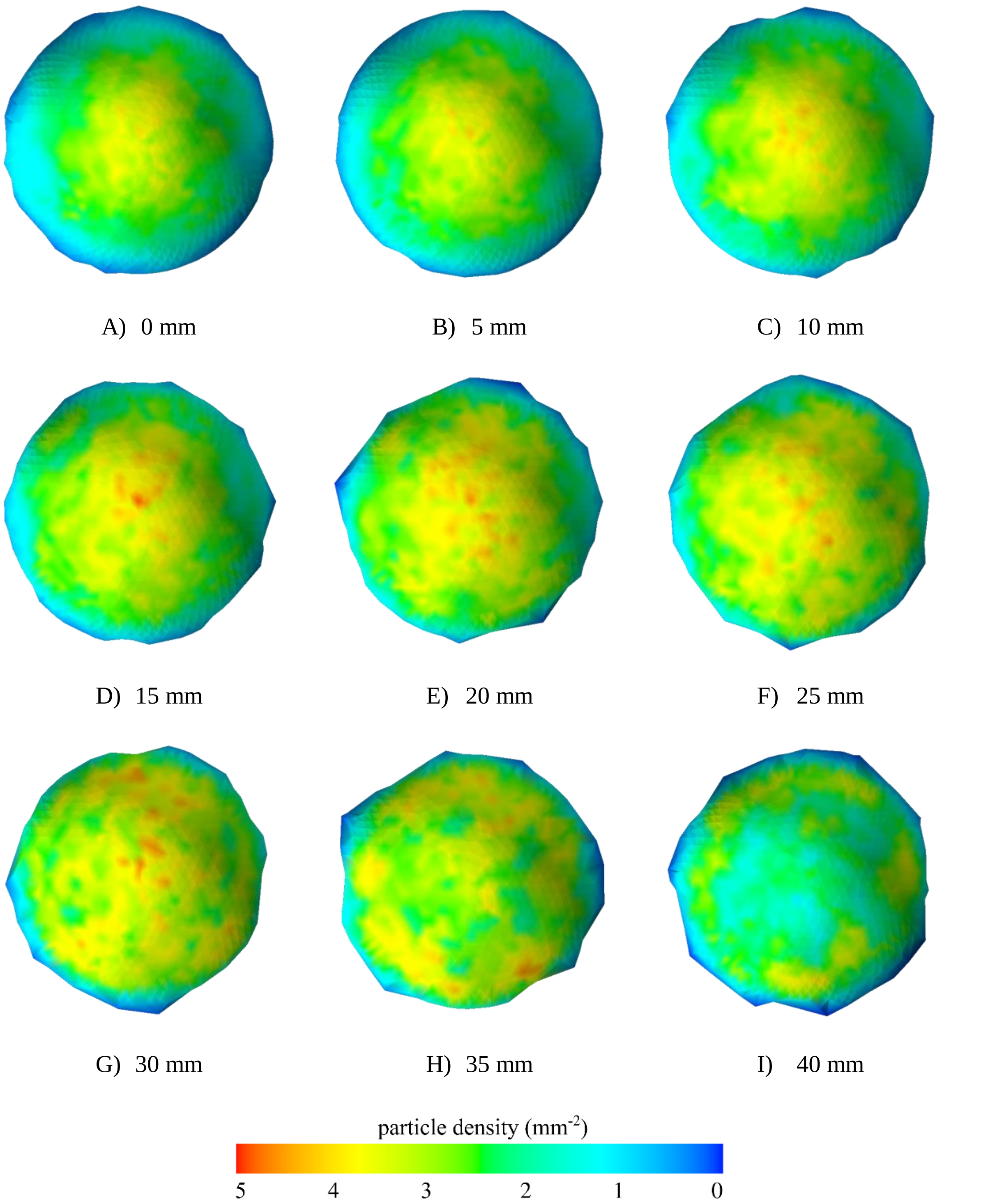

FIG S7: Simulated particle density on the sample's surface using hollow cylinders with different heights (local particle density of the implanted ions represented by colour scale).

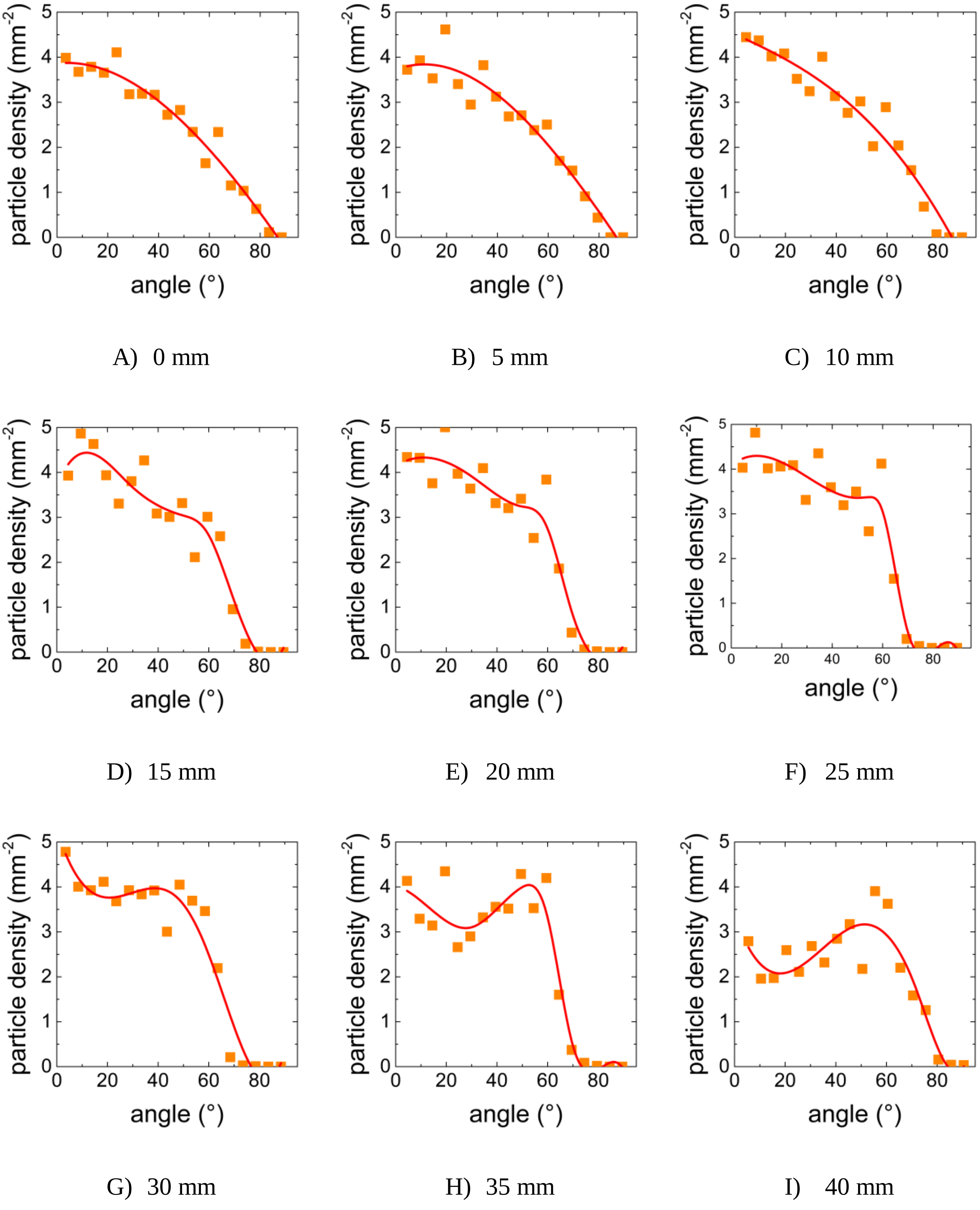

FIG S2: Simulated particle density on the sample's surface depending on the position using hollow cylinders with different heights: if no cylinder is used (0 mm case), the radial decrease is clearly visible. With increasing height of the cylinder, the "plateau" is getting broader and flatter until a height of 30 mm. Above that value, shadowing occurs.

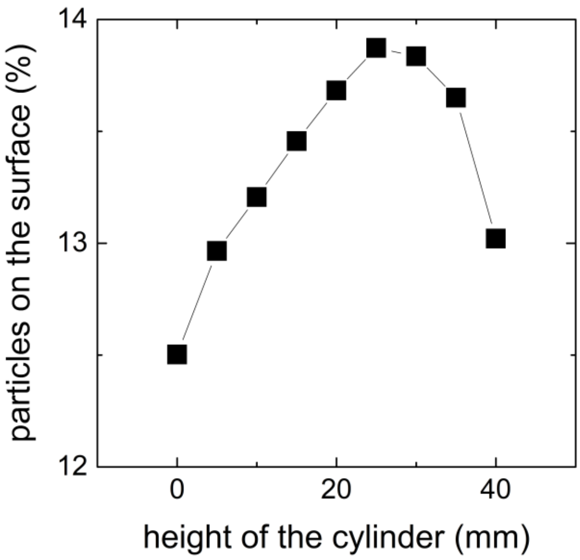

FIG S3: Share of the particles ending on the inner surface of the inlay (compared to the total number of accelerated particles) depending on the height of the attached hollow cylinder. Above 30 mm cylinder height, shadowing occurs which is responsible for the decrease in the particle number.

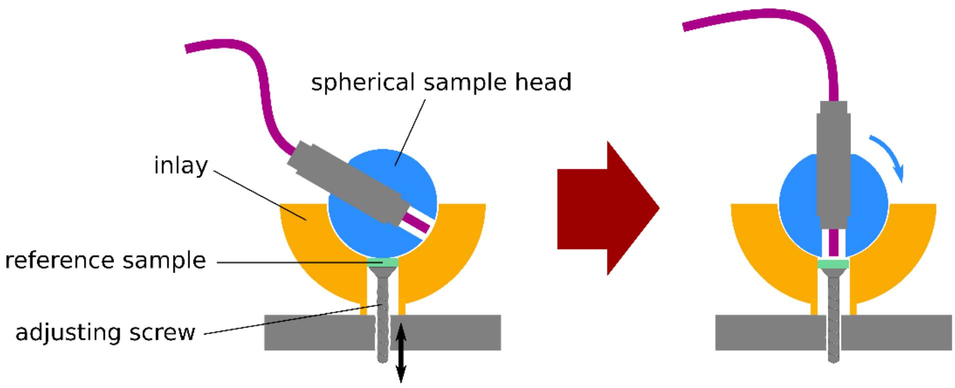

FIG S4: Calibration apparatus using reference samples with known fluence: Each sample can be moved up until it touches the sample head. By turning the head, a reflectivity measurement can be performed ensuring a fixed distance between the optical fibre and the sample's surface. The result is a calibration curve which is utilized for the conversion of the measurement data into fluence values.